Desalination and Water Treatment
www.deswater.com

doi: 10.5004/dwt.2021.27586

235 (2021) 200–208
September

Sm-doped TiO_2 with boosted photocatalytic detoxification activity benefited from the accelerated separation of photogenerated carriers

Yanbai Chen[a], Lei Wang[b], Junbo Zhong[a,b,*], Minjiao Li[a,*], Huajun Fan[a], Congxue Tian[c]

[a]*School of Chemical Engineering, Sichuan University of Science and Engineering, Zigong 643000, China, emails: junbozhong@suse.edu.cn (J. Zhong), lmj0621@126.com (M. Li), 402567598@qq.com (Y. Chen), 1464969820@qq.com (H. Fan)*
[b]*School of Chemistry and Environmental Engineering, Sichuan University of Science and Engineering, Zigong 643000, China, email: 1227443879@qq.com*
[c]*Sichuan Key Laboratory of Comprehensive Utilization of Vanadium and Titanium Resources, Panzhihua University, Panzhihua 617000, China, email: 515884764@qq.com*

Received 26 December 2020; Accepted 7 July 2021

ABSTRACT

In this study, Sm-doped TiO_2 was fabricated by a sol–gel approach. The samples were examined by some analytic techniques. The results demonstrate that Sm^{3+} exists in TiO_2, proven by energy-dispersive X-ray spectroscopy and X-ray photoelectron spectroscopy. Doping Sm into TiO_2 affects the crystal growth and optical capacity of the samples, promotes the separation of photogenerated carriers and increases the content of oxygen vacancies in the sample, boosting the visible-light-driven photocatalytic activity of the sample. Activities of the photocatalysts were investigated by detoxification of Rhodamine B under UV and visible light irradiation. All the Sm-doped TiO_2 samples possess high catalytic activity than TiO_2. When the molar ratio of Sm/Ti is 0.6%, the photocatalyst displays the highest activity, which is 6.2 times higher than that of TiO_2 and even better than commercial TiO_2 (P25) under visible light illumination. This study demonstrates that doping Sm into TiO_2 is a viable strategy to boost the photoactivity of TiO_2.

Keywords: Semiconductors; TiO_2; P25; Sm doping; Photocatalytic activity; Oxygen vacancies

1. Introduction

Water pollution is a hazard to human health and social development. Therefore, the development of effective measures to remove water contaminants remains a constant challenge. Nowadays, many reliable strategies for pollutants removal have been developed and achieved reasonable results. Among them, semiconductor-based photocatalysis has attracted considerable attention thanks to its low cost, no secondary pollution, environmentally friendly and high efficiency [1,2]. Amongst the photocatalysts developed, TiO_2 has been widely used in the photocatalytic field benefited from its long-term chemical stability, low cost, non-toxicity, high oxidizing capacity and Lewis acidity [3,4]. However, rapid recombination of the photoactivated carriers hinders the catalytic efficiency [5–9]. Thereby, it is critical to boosting the partition of photoexcited carriers, ameliorating the photocatalytic activity of TiO_2. Studies show that doping is a reliable strategy to inhibit the reunion of photoactivated charge pairs by altering the electric structures of TiO_2 [10–18], subsequently influencing the segregation of photoinduced carriers.

As a kind of rare earth metal, Sm can act as catalysts or dopant due to incompletely occupied 4f orbitals and empty 5d orbitals. At the same time, the separation efficiency of photogenerated carriers can be improved by forming a new energy level after doping Sm into TiO_2, therefore, photons with less energy can excite the electrons to the

* Corresponding authors.

new energy levels, thus improving light response capacity. Sm^{3+} ion contains intra-4f orbital, which can influence the electric structures of TiO_2, therefore it is anticipated that doing Sm into TiO_2 can improve the separation of photoactivated carriers. Ramesan et al. studied and reported that Sm doping could affect the photocatalytic activity of TiO_2 [19,20]. However, the effect of Sm doping on the photogenerated carriers separation efficiency of TiO_2 and oxygen vacancies (OVs) produced have been seldom concerned, since separation efficiency of photogenerated carriers and OVs produced can definitely influence the catalytic performance, it is absolutely necessary to study these two factors to reveal how separation efficiency of photogenerated carriers and OVs affect the catalytic activity.

Various methods are employed to dope elements into photocatalysts, such as baking in the atmosphere [7,21], a hydrothermal method [21,22], magnetron sputtering [23,24], precipitation method [25,26] and so on. Among the doping methods developed, sol–gel approach is a facile and reliable strategy. Sol–gel approach can precisely control the composition, possessing low equipment cost [27]. Therefore, sol–gel method is widely employed to dope ions into photocatalysts [28–31].

Herein, to investigate the effects of doping Sm into TiO_2 on the separation behaviors of photoexcited carriers and photocatalytic properties, we fabricated Sm-doped TiO_2 via a sol–gel strategy. The photocatalysts were characterized by X-ray diffractometer (XRD), scanning electron microscope (SEM) with energy-dispersive X-ray spectroscopy (EDS), X-ray photoelectron spectroscopy (XPS), surface photovoltage spectrum (SPS) and electron spin resonance (ESR). The existence of Sm in TiO_2 was confirmed by XPS and EDS. Photocatalytic activity of the samples was evaluated by detoxification of Rhodamine B (RhB) under UV and visible light irradiation, the outcomes reveal that Sm-doped TiO_2 displays higher activity than the undoped TiO_2 due to higher separation rate of photoinduced carriers, proven by SPS observation.

2. Experimental section

2.1. Preparation of Sm-doped TiO_2

Sm-doped TiO_2 was prepared by a sol–gel method as the recipe described by the study of Mohammed [32]. 3 mL $Sm(NO_3)_3$ aqueous solution was introduced into the sol–gel system. The molar ratio of Sm/Ti is 0.2%, 0.4%, 0.6%, 0.8% and 1.0%, respectively. All the powder samples were calcinated at 723 K for 2 h. Sm-doped TiO_2 was designed as 0.2%, 0.4%, 0.6%, 0.8% and 1.0%, respectively. The undoped TiO_2 was allocated as 0%.

2.2. Characterization of the samples

The texture properties of the samples were analyzed on a SSA-4200 specific surface analyzer. The crystal structure of the catalysts was identified on a DX-2600 X-ray diffractometer. The microstructures of the samples were observed on a VEGA3 SBU SEM with EDS. The light-responsive capacity was measured on a UH-4150 UV-Vis spectrophotometer. XPS was performed on a XSAM 800 X-ray photoelectron spectrometer. SPS was executed on a homemade apparatus. OVs were investigated on an electron spin resonance (ESR, Bruker A300). The yield of $^{\bullet}O_2^-$ was quantitatively compared by nitrotetrazolium blue chloride (NBT)-superoxide radical ($^{\bullet}O_2^-$) exclusive reaction [33], low concentration after irradiation indicates a high yield of $^{\bullet}O_2^-$ generated in the photocatalytic reaction system.

2.3. Photocatalytic reaction

The activity of the catalysts was assessed by decontamination of 50 mL RhB solution under a 500 W high-pressure mercury lamp shine/visible light irradiation, visible light was provided by a 300 W Xenon lamp with a 420 nm cutoff filter. The concentration of RhB and photocatalyst is 10 mg/L and 1 g/L, separately. Before photocatalytic reaction, the suspension system was intensely stirred in dark for 20 min, the adsorption–desorption equilibrium can be established after 20 min.

To discern the type and role of the active radicals for the destruction of RhB, 2 mL isopropanol (IPA, 5 mmol/L) as hydroxyl radical ($^{\bullet}OH$) scavengers, 2 mL ammonium oxalate (AO, 5 mmol/L) as hole (h^+) scavengers and 2 mL benzoquinone (BQ, 5 mmol/L) as superoxide radical ($^{\bullet}O_2^-$) scavengers were added into the reaction system [34–36], low decay efficiency of RhB corresponds to strong inhibition effect of scavenger, consequently revealing the leading role of the specific active radicals.

3. Results and discussion

3.1. Characterization of the photocatalysts

To reveal the effects of doping Sm into TiO_2 on the crystal growth of TiO_2, a specific surface area measurement was performed. The surface area for 0%, 0.2%, 0.4%, 0.6%, 0.8% and 1.0% is 71.8, 78.4, 85.2, 92.4, 96.2 and 105 m^2/g, separately. Distinctly, all the Sm-doped samples exhibit a higher specific surface than the undoped TiO_2, demonstrating that doping a low amount of Sm^{3+} into TiO_2 can remarkably alter the surface area of TiO_2. Evidently, Sm^{3+} inhibits the crystal growth of TiO_2, reducing the crystallinity and producing more defects. Similar results were acquired when Ag^+ was doped into TiO_2 [37]. Commonly, low crystallinity can offer a high surface area, which can provide more active sites for the catalytic reaction. The introduction of suitable defects can facilitate the separation of carriers, heightening the photoactivity [38–41], which can be confirmed by results of low-temperature ESR and photocatalysis.

XRD profiles of the samples fabricated are depicted in Fig. 1A and B, all the diffraction peaks can be indexed as the anatase-type TiO_2 (JCPDS No. 89–4921) [31]. For Sm-doped TiO_2, no peaks for Sm_2O_3 were detected owing to the low loading of Sm^{3+}. Notably, Sm-doped TiO_2 catalysts appear broader diffraction peak than the reference TiO_2, which solidly suggests that Sm-doped TiO_2 catalysts have a smaller crystal size than TiO_2 according to the Debye–Scherrer equation. The average crystal size of the 0%, 0.2%, 0.4%, 0.6%, 0.8% and 1.0% sample is 12.8, 11.5, 11.1, 8.1, 8.0 and 6.7 nm, respectively. This smaller crystal size of the catalyst is consistent with a high specific surface

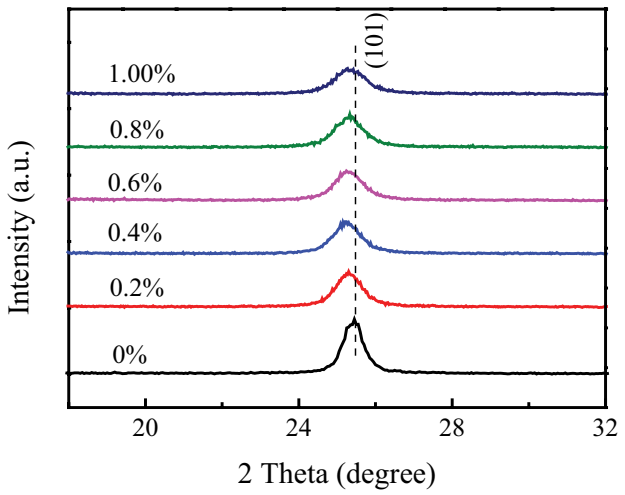

Fig. 1. Crystal structures of the samples, the enlargement of the (101) plane of the samples.

area, which is in good harmony with the measurement of surface area. Fig. 1B demonstrates that the diffraction peaks of the (101) plane of Sm-doped TiO_2, which shows a shift to a lower angle. This is probably caused by the doping with Sm ions. The results suggest the existence of Sm^{3+} in TiO_2. The ionic radius of Ti^{4+} is 0.065 nm, while for Sm^{3+}, the ionic radius is 0.0958 nm. The doping of Sm^{3+} increases the unit cell, resulting in change towards the smaller 2θ. Similar results were observed when Re^{4+} was doped into TiO_2 [42]. XRD results confirm that Sm influences the crystal structure of TiO_2, inevitably affecting the separation of carriers and photocatalytic activity of TiO_2.

SEM of the samples are illustrated in Fig. 2A and B. Two samples exhibit lump-like shape, indicating that small loading of Sm^{3+} cannot effectively alter the shape of TiO_2, the shape of TiO_2 is mainly determined by the sol–gel process and baking temperature. Fig. 2C–E show element mappings of the 0.6% sample, evidently, O, Ti and Sm were detected, which further proves that Sm doped TiO_2 was successfully prepared. The existence of Sm in TiO_2 can be further supported by XPS results.

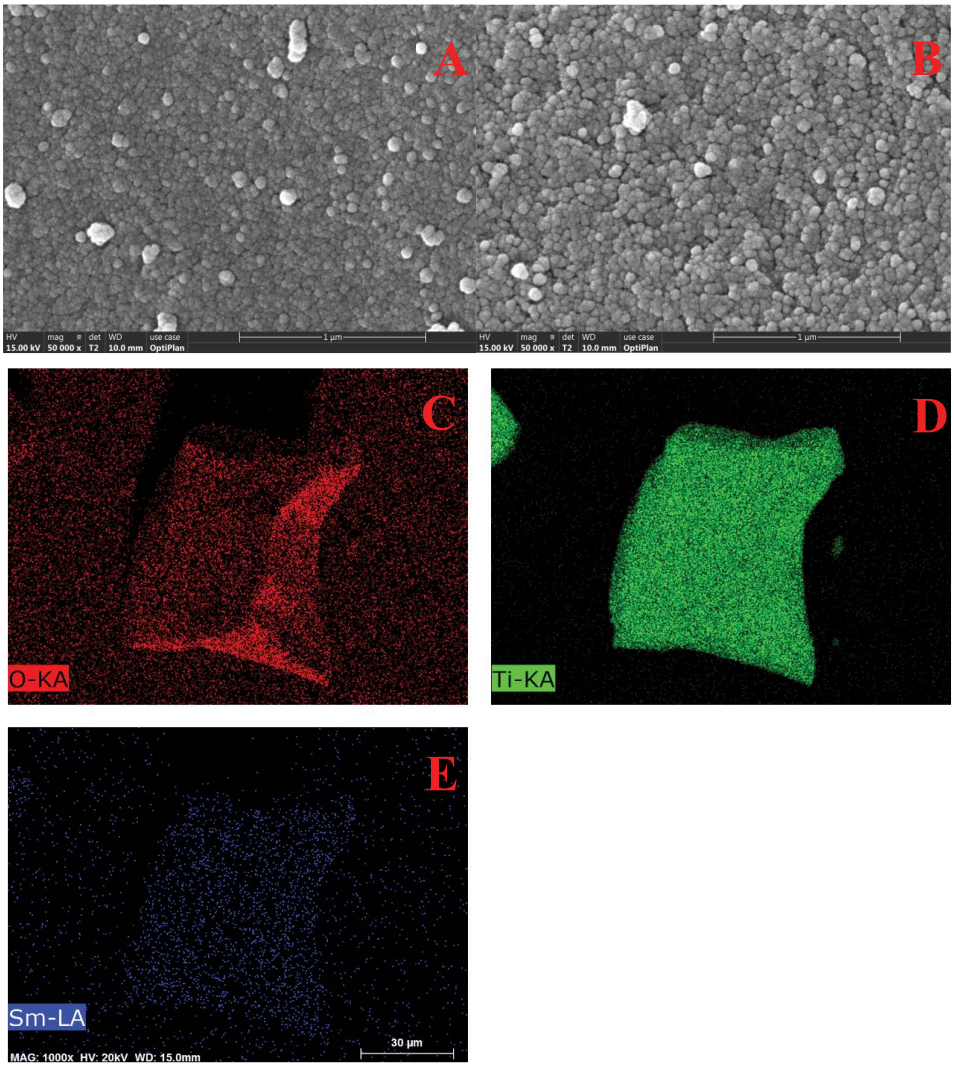

Fig. 2. SEM information of the samples (A) 0%, (B) 0.6%, element mapping of the 0.6% sample (C).

Light absorption capacity is vital for the generation of active radicals, which performs a significant role in destructing of decontaminants, therefore it is crucial to study the light response properties of the samples prepared. Fig. 3A is the light response capacity of the samples. The results show that Sm-doped TiO_2 appears to promote light absorbance ability in the visible light region as the loading of Sm elevating [43,44]. As shown in Fig. 3B, the bandgap of the samples can be estimated by the following formula: E_g = 1,240/l [45]. The bandgap of the reference TiO_2 is 2.93 eV, the bandgap of Sm-doped samples is about 2.97 eV, the valence band (VB) and conduction band (CB) band edge potential of the reference TiO_2 and the Sm doped TiO_2 can be obtained by the formula: $E_{VB} = X - E^e + 0.5E_g$, $E_{CB} = E_{VB} - E_g$ [46], respectively. Where E_{CB} and E_{VB} are CB and VB band edge potential, respectively, X is the absolute electronegativity of semiconductors, and E^e is the energy of free electrons on the hydrogen scale (about 4.5 eV) [47]. The value of X for TiO_2 is 5.78 eV [48]. Therefore, E_{VB} and E_{CB} of TiO_2 is 2.75 and –0.19 eV, respectively, and E_{VB} and E_{CB} of Sm doped TiO_2 is 2.77 and –0.205 eV, respectively.

To figure out the surface state and micro-environment, XPS analysis was carried out. Fig. 4A is high-resolution XPS spectra of Ti $2p_{1/2}$, it is evident that the binding energy of Ti $2p_{1/2}$ shifts to a lower value. The ionic radii of Sm^{3+} (0.0958 nm) are greater than Ti^{4+} (0.065 nm), therefore only a little amount of Sm^{3+} enters the crystal lattice of TiO_2 by replacing the Ti^{4+} ions, inducing the shift of binding energy of Ti $2p_{1/2}$. Fig. 4B is the high-resolution XPS spectra of Sm 3d, the peak at 1083.0 eV can be attributed to the binding energy of Sm^{3+}. XPS characterization results definitely confirm the existence of Sm in TiO_2. The existence of Sm in TiO_2 will inevitably influence the separation of photogenerated carriers.

SPS is an available technology to reveal the separation behavior of the photoexcited carriers. The SPS results are demonstrated in Fig. 6. It is apparent that all the samples display obvious SPS response from 300–400 nm, no detectable SPS signals were observed in the visible light region, which accords well with the bandgap of the samples. Interestingly, all the Sm-doped samples exhibit stronger SPS response than the undoped TiO_2, affirming that Sm doping promotes the separation of photoinduced carriers, among all the samples, the 0.6% sample has the strongest SPS response. In light of the measurement principle of SPS, strong SPS signals demonstrate a high separation rate of

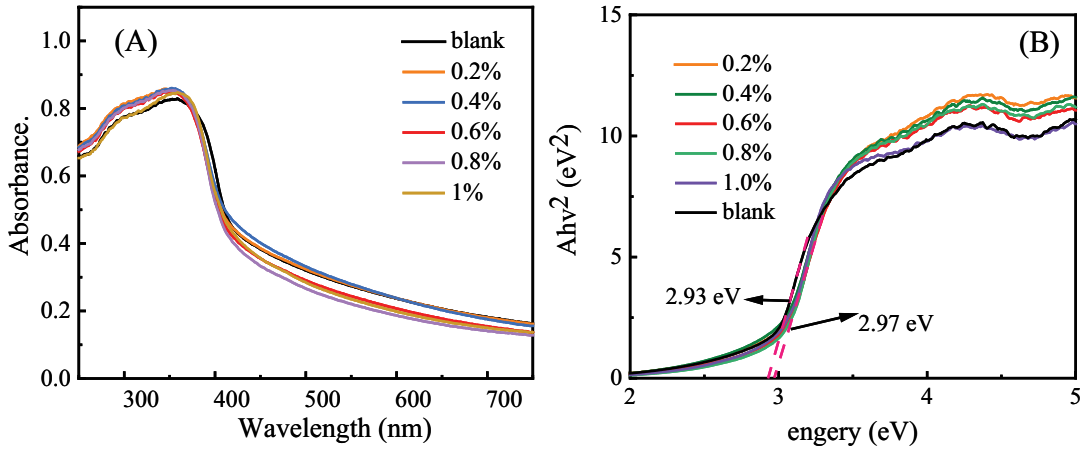

Fig. 3. (A) Light response capacity of the samples and (B) bandgap of the samples.

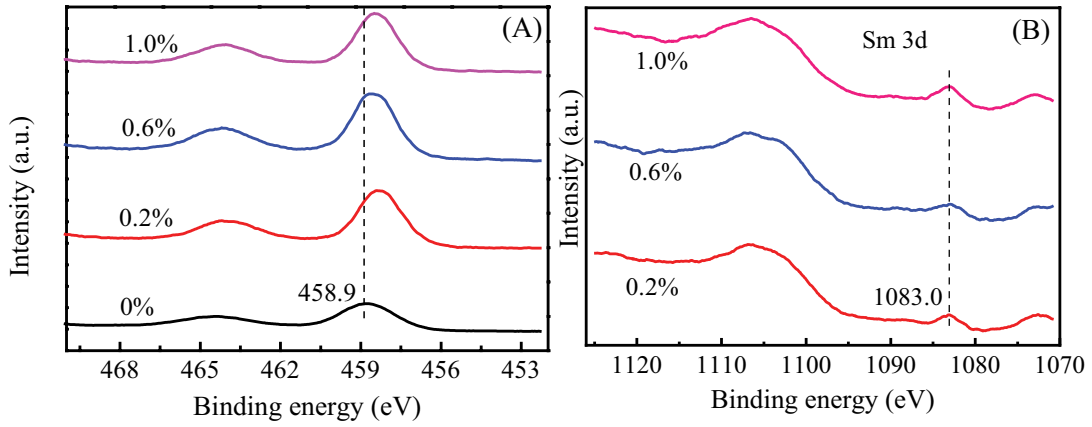

Fig. 4. (A) High-resolution Ti 2p of the samples and (B) high-resolution Sm 3d of the samples.

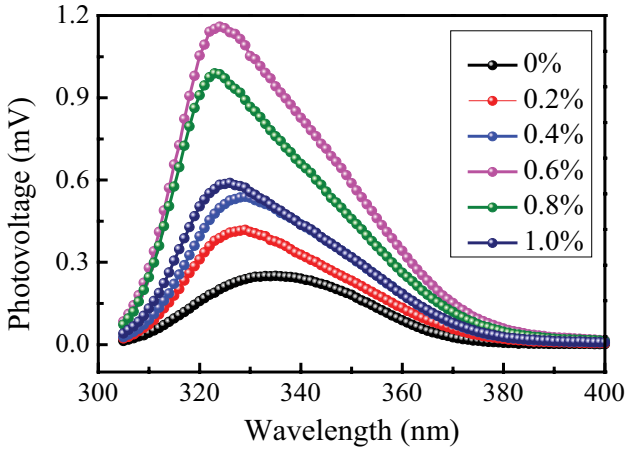

Fig. 5. SPS results of the samples.

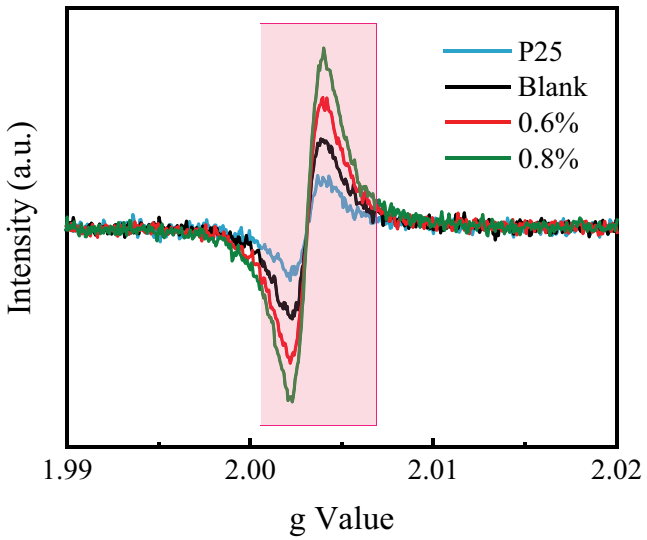

Fig. 6. Low temperature ESR signals of the samples (0%, 0.6%, 0.8%, P25).

photoinduced carriers [49], consequently, the 0.6% sample has the highest separation rate of carriers. The results further demonstrate the high concentration of Sm^{3+} will inhibit the separation of carriers, a relatively high level of Sm^{3+} will be the recombination centers of electrons and holes, resulting in a weak SPS response. Although relatively high Sm^{3+} dopant will exhibit a low separation rate of carriers, the separation rate of photogenerated carriers of 1.0% is still higher than the reference TiO_2. It is commonly acknowledged that the separation rate of photogenerated carriers plays a leading role in influencing the activity of photocatalysts [26,50], thereby it is anticipated that the 0.6% sample will display the highest photocatalytic activity.

OVs are defects induced by O atom deficiency in the lattice. OVs are catalytic centers for the activation of O_2, and the appropriate amount of OVs can promote the generation of $^{\bullet}O_2^-$ [51]. OVs can form a new energy level between CB and VB. TiO_2 only can be excited by ultraviolet light. However, due to the introduction of OVs, a new energy level can be formed. O_2 can also be captured by OVs, then $^{\bullet}O_2^-$ can be formed by assuming electrons, accelerating the yield of $^{\bullet}O_2^-$ and participating in the reaction [52]. Consequently, photocatalysts with OVs will display visible-light-driven photocatalytic activity. As active species, a high level of $^{\bullet}O_2^-$ will boost the activity of photocatalysts, therefore, it is significant to study the OVs induced by Sm doping. Fig. 6 is low-temperature ESR results of TiO_2 (0%), P25, 0.6% and 0.8%. The paramagnetic signal at g = 2.004 can be allocated to OVs generated by Zeeman Effect [53]. It is apparent that TiO_2 (0%), P25, 0.6% and 0.8% all have OVs, which indicates that the reference TiO_2 (0%), P25, 0.6% and 0.8% will exhibit visible light-responsive photocatalytic activity. Moreover, ESR signals of the 0.6% sample are stronger than other samples, which firmly indicates that the 0.6% sample produces more OVs. High OVs is beneficial to yield $^{\bullet}O_2^-$, which can be supported by NBT observation. The result further demonstrates that excessive Sm results in a low level of OVs, the mechanism needs to be further revealed in near future.

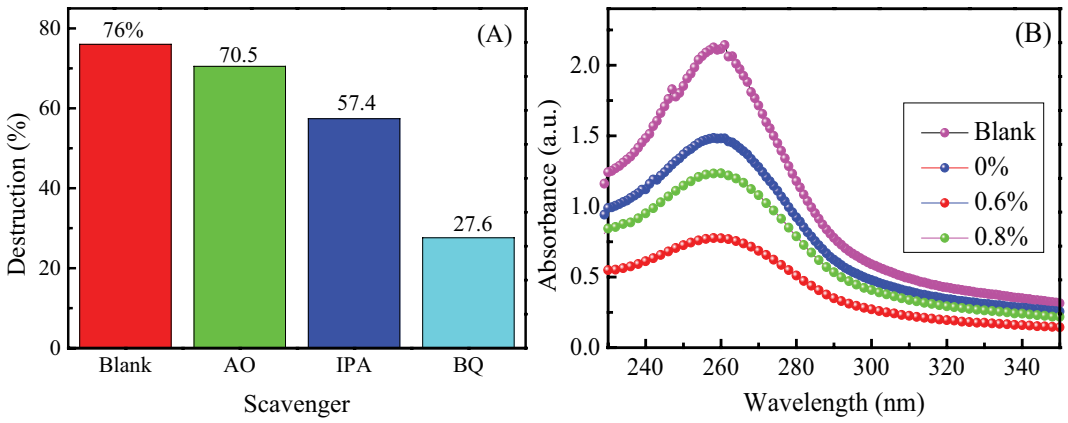

Fig. 7. (A) Destruction of RhB with the existence of the different scavengers (adsorption in dark for 20 min; irradiation time = 20 min; the concentration of scavenger is 0.2 mmol/L) and (B) absorbance of NBT in the different photocatalytic reaction systems (irradiation time = 20 min; NBT dosage = 0.05 mmol/L).

Trapping experiment is a valid method to reveal the role of active species in the photocatalytic reaction. Scavengers can quench the active radicals, resulting in the low catalytic activity of the photocatalyst. The results of the trapping experiment are exhibited in Fig. 7A. With the existence of BQ in the photocatalytic reaction system, the destruction efficiency of RhB drops from 76% to 27.6%, firmly certifying that $^{\bullet}O_2^-$ exists in the photocatalytic reaction system and $^{\bullet}O_2^-$ takes a leading role in abating of RhB, coinciding well with OVs characterization. In addition, $^{\bullet}OH$ performs a secondary role, while the role of h^+ is minor. E_{VB} of the 0.6% is 2.77 eV, holes can oxidize H_2O/OH^- to form $^{\bullet}OH$. As strong oxidants are produced $^{\bullet}OH$ radicals can oxidize the pollutants. Besides, holes also can directly oxidize organic pollutants. However, the oxidation capacity of $^{\bullet}OH$ is stronger than h^+, therefore, holes perform a minor role for the photoactivity.

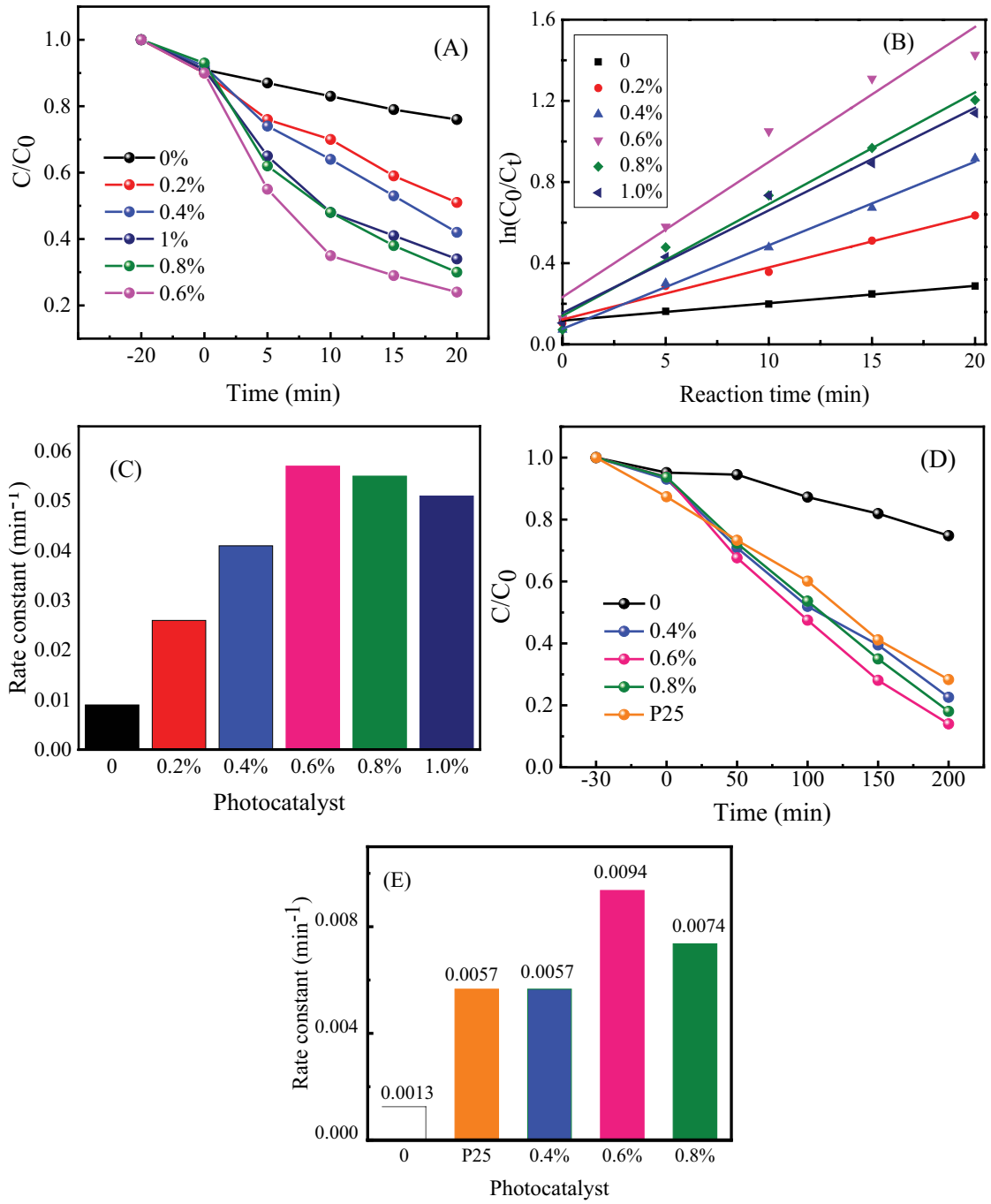

Fig. 8. (A) Photocatalytic decontamination of RhB on the different samples, (B) relationship between $\ln(C_0/C_t)$ and irradiation time, (C) destruction rate constants of RhB over the different samples, (D) photocatalytic decontamination of RhB on the different samples under visible light irradiation and (E) destruction rate constants of RhB over the different samples under visible light irradiation.

To further compare the level of $^{\bullet}O_2^-$, NBT-$^{\bullet}O_2^-$ measurements were performed. As shown in Fig. 7B, the absorbance of NBT in the Sm-TiO_2 system is lower than that in TiO_2 catalytic system, and the 0.6% catalytic system generates the highest $^{\bullet}O_2^-$ given the NBT-$^{\bullet}O_2^-$ reaction theory. The observation firmly demonstrates that doping Sm into the TiO_2 expedites the yield of $^{\bullet}O_2^-$. As active species with strong oxidation capacity, a high level of $^{\bullet}O_2^-$ can heighten the decontamination of pollutants, thereby the photocatalyst displays high photocatalytic activity.

3.2. Photocatalytic evaluation

Doping Sm into TiO_2 influences the crystal growth and boosts the separation of photoinduced carriers, it is anticipated that Sm-doped TiO_2 will display higher activity towards the destruction of pollutants. To confirm this idea, photocatalytic properties of the samples were evaluated by degradation of RhB. Fig. 8A shows the destruction of RhB on the samples, it is apparent that the removal of RhB is photocatalysis and the destruction of RhB on all the Sm-doped samples is faster than that on the reference TiO_2, the 0.6% sample exhibits the highest activity. To further compare the photocatalytic activity of the samples, the results in Fig. 8A were analyzed. $\ln(C_0/C_t) = kt$ can well describe the trend of photocatalytic abatement of RhB, where C_0 is the concentration of RhB before irradiation, while C_t is the concentration of RhB after illumination, k is the rate constant of RhB over the samples. The relationship between $\ln(C_0/C_t)$ and t is provided in Fig. 8B, it is evident that $\ln(C_0/C_t) = kt$ can well represent the degradation of RhB over the samples, and the corresponding destruction rate constants of RhB on the samples are shown in Fig. 8C. All Sm-doped TiO_2 photocatalysts exhibit higher activity than the 0%, the activity of Sm-doped TiO_2 gradually boosts as the loading of Sm increasing, and the 0.6% sample has the highest activity. However, the activity of Sm-doped TiO_2 tends to descend, which suggests that relatively high loading of Sm is not conducive to the activity of the sample. Even though, the activity of the 1.0% sample is still higher than the reference TiO_2. For the 0.6% sample, the photocatalytic performance is more than 6 times that of the 0% sample. Such enhancement in photocatalytic activity suggests that doping Sm into TiO_2 can significantly improve the photocatalytic activity of TiO_2. To further evaluate photocatalytic activity of Sm-doped TiO_2 photocatalysts, destruction of RhB under visible light irradiation was performed. Fig. 8D and E show that the 0.6% sample still has the highest activity with visible light, the activity of the 0.6% sample is higher than commercial TiO_2 (P25). The photocatalytic performance of 0.6% is more than 7.2 times that of 0% and 1.6 times that of P25 with visible light. The results definitely demonstrate that doping Sm into TiO_2 is a robust channel to boost the activity of TiO_2. As shown in Fig. 6, the level of OVs on the 0.6% and the 0.8% samples is significantly increased compared to that on the 0% sample. The relevant literature has confirmed that the introduction of a suitable amount of OVs results in the formation of a new energy level between VB and CB, promoting the visible light response. The electrons on the new energy level can accelerate photogenerated charge separation and react with O_2 to generate $^{\bullet}O_2^-$ [54–56]. In this work, the introduction of OVs endows Sm-doped TiO_2 with higher visible light activity than P25 and the reference TiO_2.

4. Conclusions

In this work, we prepared Sm-doped TiO_2 by a sol–gel approach with Sm doping concentrations from 0.2%–1.0%. The existence of Sm in TiO_2 inhibits the crystal growth of TiO_2, boosting the specific surface area. The low-temperature ESR spectra reveal that doping Sm into TiO_2 generates defects in the samples, which promotes the segregation of photoinduced carriers and subsequently boosts the formation of $^{\bullet}O_2^-$. Degradation of RhB over Sm doped TiO_2 is faster than that over the reference TiO_2, and the 0.6% shows the highest photocatalytic activity. Doping Sm introduces more oxygen vacancies into the sample, the introduction of oxygen vacancies endows Sm-doped TiO_2 samples with visible-light-driven photocatalytic activity. This study demonstrates that doping Sm into TiO_2 is a reliable strategy to improve the photocatalytic activity of TiO_2.

Acknowledgments

We are grateful to Science and Technology Department of Sichuan Province (No. 2019YJ0457, No. 2019ZYZF0069) and Sichuan Key Laboratory of Comprehensive Utilization of Vanadium and Titanium Resources (2018FTSZ01, 2018FTSZ02, and 2018FTSZ15) for financial support.

References

[1] P. Dong, G. Hou, X. Xi, R. Shao, F. Dong, WO_3-based photocatalysts: morphology control, activity enhancement and multifunctional applications, Environ. Sci. Nano, 4 (2017) 539–557.
[2] T. Zadi, M. Aziz, N. Nasrallah, A. Bouzaza, R. Maachi, D. Wolbert, S. Rtimi, A.A. Assadi, Indoor air treatment of refrigerated food chambers with synergetic association between cold plasma and photocatalysis: process performance and photocatalytic poisoning, Chem. Eng. J., 382 (2020) 122951, doi: 10.1016/j.cej.2019.122951.
[3] M.H. Geesi, O. Ouerghi, A. Elsanousi, A. Kaiba, Y. Riadi, Ultrasound-assisted preparation of Cu-doped TiO_2 nanoparticles as a nanocatalyst for sonochemical synthesis of pyridopyrimidines, Polycyclic Aromat. Compd., (2020), doi: 10.1080/10406638.2020.1716029.
[4] D. Tekin, D. Birhan, H. Kiziltas, Thermal, photocatalytic, and antibacterial properties of calcinated nano-TiO_2/polymer composites, Mater. Chem. Phys., 251 (2020) 123067, doi: 10.1016/j.matchemphys.2020.123067.
[5] X. Qu, Y. Yi, F. Qiao, M. Liu, X. Wang, R. Yang, H. Meng, L. Shi, F. Du, TiO_2/BiOI/CQDs: enhanced photocatalytic properties under visible-light irradiation, Ceram. Int., 44 (2018) 1348–1355.
[6] A. Meng, L. Zhang, B. Cheng, T. Yu, TiO_2–MnO_X–Pt hybrid multiheterojunction film photocatalyst with enhanced photocatalytic CO_2-reduction activity, ACS Appl. Mater. Interfaces, 11 (2019) 5581–5589.
[7] J. Huang, L. Dou, J. Li, J. Zhong, M. Li, T. Wang, Excellent visible light responsive photocatalytic behavior of N-doped TiO_2 toward decontamination of organic pollutants, J. Hazard. Mater. 403 (2021) 123857, doi: 10.1016/j.jhazmat.2020.123857.
[8] X. Cheng, Y. Shang, Y. Cui, R. Shi, Y. Zhu, P. Yang, Enhanced photoelectrochemical and photocatalytic properties of anatase-TiO_2(B) nanobelts decorated with CdS nanoparticles, Solid State Sci., 99 (2020) 106075, doi: 10.1016/j.solidstatesciences.2019.106075.

[9] J. Huang, H. Liu, J. Li, J. Zhong, T. Wang, J. Li, M. Li, Photocatalytic activity of TiO_2 prepared by different solvents through a solvothermal approach, Solid State Sci., 98 (2019) 106024, doi: 10.1016/j.solidstatesciences.2019.106024.
[10] W. Hua, F. Dong, J. Zhang, M. Liu, H. He, Y. Wu, D. Yang, H. Deng, Differently ordered TiO_2 nanoarrays regulated by solvent polarity, and their photocatalytic performances, Appl. Surf. Sci., 442 (2018) 298–307.
[11] E.I. Naik, H.S.B. Naik, R. Viswanath, I.K. Suresh Gowda, M.C. Prabhakara, Bright red luminescence emission of macroporous honeycomb-like Eu^{3+} ion-doped ZnO nanoparticles developed by gel-combustion technique, Appl. Surf. Sci., 5 (2020) 863, doi:10.1007/s42452-020-2639-x.
[12] K. Abdellah, O. Oussama, G.H. Mohammed, E. Ammar, B. Afif, D.B. Oussamaehbi, Characterization and catalytic performance of Ni-Doped TiO_2 as a potential heterogeneous nanocatalyst for the preparation of substituted pyridopyrimidines, J. Mol. Struct., 1203 (2020) 127376, doi: 10.1016/j.molstruc.2019.127376.
[13] X. Yu, J. Xie, H. Dong, Q. Liu, Y. Li, Effects of oxygen defects on electronic band structures and dopant migration in Sn-doped TiO_2 by density functional studies, Chem. Phys. Lett., 754 (2020) 137732, doi: 10.1016/j.cplett.2020.137732.
[14] V. Sarunas, M. Arturs, L. Martynas, M. Darius, A. Andris, Black carbon-doped TiO_2 films: synthesis, characterization and photocatalysis, J. Photochem. Photobiol., A, 382 (2019) 111941, doi: 10.1016/j.jphotochem.2019.111941.
[15] N. Sharotri, D. Sharma, D. Sud, Experimental and theoretical investigations of Mn-N-co-doped TiO_2 photocatalyst for visible light induced degradation of organic pollutants, J. Mater. Res. Technol., 5 (2019) 3995–4009.
[16] L. Tian, L. Xiang, X. Shen, Q. Li, S. Ge, B. Liu, L. Jie, Visible light enhanced Fe-I-TiO_2 photocatalysts for the degradation of gaseous benzene, Atmos. Pollut. Res., 11 (2020) 179–185.
[17] S. Abbad, K. Guergouri, S. Gazaout, S. Djebabra, A. Zertal, R. Barille, M. Zaabat, Effect of silver doping on the photocatalytic activity of TiO_2 nanopowders synthesized by the sol–gel route, J. Environ. Chem. Eng., 8 (2020) 103718, doi: 10.1016/j.jece.2020.103718.
[18] S. Wang, J. Wang, W. Liu, Effect of F, V and Mn co-doping on the catalytic performance of TiO_2-pillared bentonite in the photocatalytic denitration, J. Fuel Chem. Technol., 48 (2020) 1131–1139.
[19] F. Alcaide, R.V. Genova, G. Álvarez, H.-J. Grande, Ó. Miguel, P.L. Cabot, Platinum-catalyzed Nb-doped TiO_2 and Nb-doped TiO_2 nanotubes for hydrogen generation in proton exchange membrane water electrolyzers, Int. J. Hydrogen Energy, 40 (2020) 20605–20619.
[20] M.T. Ramesan, T. Sampreeth, In situ synthesis of polyaniline/Sm-doped TiO_2 nanocomposites: evaluation of structural, morphological, conductivity studies and gas sensing applications, J. Mater. Sci.: Mater. Electron., 29 (2017) 4301–4311.
[21] T. Xia, X. Chen, Revealing the structural properties of hydrogenated black TiO_2 nanocrystals, J. Mater. Chem., 1 (2013) 2983–2989.
[22] F. Mokhtari, N. Tahmasebi, Hydrothermal synthesis of W-doped BiOCl nanoplates for photocatalytic degradation of Rhodamine B under visible light, J. Phys. Chem. Solids, 149 (2020) 109804, doi: 10.1016/j.jpcs.2020.109804.
[23] J. Zhong, J. Chen, Q. Yang, C. Hu, J. Li, R. Duan, Remarkably enhanced photoinduced charge separation rate of Bi_2WO_6 by Cu^{2+} doping, Appl. Phys. A, 124 (2018) 583–589.
[24] A.K. Yadav, S.H. Maidul, D.K. Shukla, D.M. Phase, S.N. Jha, D. Bhattacharyy, Local structural investigations of Fe-doped TiO_2 amorphous thin films, Thin Solid Films, 716 (2020) 138435, doi: 10.1016/j.tsf.2020.138435.
[25] A. Dziedzic, W. Bochnowski, S. Adamiak, L. Szyller, J. Cebulski, I. Virt, M. Kus-Liśkiewicz, M. Marzec, P. Potera, A. Żaczek, B. Zdeb, Structure and antibacterial properties of Ag and N doped titanium dioxide coatings containing $Ti_{2.85}O_4N$ phase, prepared by magnetron sputtering and annealing, Surf. Coat. Technol., 393 (2020) 125844, doi: 10.1016/j.surfcoat.2020.125844.
[26] D.K. Reshma, M.K. Rajbhar, A. Ashina, E. Ramasamy, S. Mallick, T.N. Rao, G. Veerappan, A facile co-precipitation method for synthesis of Zn doped $BaSnO_3$ nanoparticles for photovoltaic application, Mater. Chem. Phys., 258 (2021) 123939, doi: 10.1016/j.matchemphys.2020.123939.
[27] N.F. Andrade, L.E. Nascimento, M. Correa, F. Bohn, M.R.D. Bomio, F.V. Mott, Characterization and photocatalytic application of Ce4p, Co2p, Mn2p and Ni2p doped Fe_3O_4 magnetic nanoparticles obtained by the co-precipitation method, Mater. Chem. Phys., 242 (2020) 122489.
[28] J. Zhong, J. Li, X. He, J. Zeng, Y. Lu, W. Hu, K. Lin, Improved photocatalytic performance of Pd-doped ZnO, Curr. Appl. Phys., 12 (2012) 998–1001.
[29] E.I. Naik, H.S.B. Naik, R. Viswanath, B.R. Kirthan, M.C. Prabhakara, Effect of zirconium doping on the structural, optical, electrochemical and antibacterial properties of ZnO nanoparticles prepared by sol–gel method, Chem. Data Collect., 29 (2020) 100505, doi: 10.1016/j.cdc.2020.100505.
[30] T. Hussain, M. Junaid, H.A. Qayyum, Preparation of Ba-doped $SrTiO_3$ photocatalyst by sol–gel method for hydrogen generation, Chem. Phys. Lett., 754 (2020) 137741, doi: 10.1016/j.cplett.2020.137741.
[31] M. Sankar, M. Jothibas, A. Muthuvel, A. Rajeshwari, S. Johnson, Structural, optical and photocatalytic degradation of organic dyes by sol gel prepared Ni doped CdS nanoparticles, Surf. Interfaces, 21 (2020) 100775, doi: 10.1016/j.surfin.2020.100775.
[32] M.K.A. Mohammed, Sol–gel synthesis of Au-doped TiO_2 supported SWCNT nanohybrid with visible-light-driven photocatalytic for high degradation performance toward methylene blue dye, Optik, 223 (2020) 165607, doi: 10.1016/j.ijleo.2020.165607.
[33] J. Zhong, J. Li, F. Feng, S. Huang, J. Zeng, CTAB-assisted fabrication of TiO_2 with improved photocatalytic performance, Mater. Lett., 100 (2013) 195–197.
[34] J. Huang, H. Liu, J. Zhong, J. Li, Enhanced simulated sunlight-driven photocatalytic performance of $SnWO_4$ prepared in the presence of cetyltrimethylammonium bromide, Environ. Prog. Sustainable Energy, 39 (2020) e13314, doi: 10.1002/ep.13314.
[35] J. Huang, H. Liu, J. Chen, J. Zhong, J. Li, R. Duan, In-situ loading of $(BiO)_2CO_3$ on g-C_3N_4 with promoted solar-driven photocatalytic performance originated from a direct Z-scheme mechanism, Mater. Sci. Semicond. Process., 82 (2018) 97–103.
[36] P. Chen, F. Wang, Z. Chen, Q. Zhang, Y. Su, L. Shen, K. Yao, Y. Liu, Z. Cai, W. Lv, G. Liu, Study on the photocatalytic mechanism and detoxicity of gemfibrozil by a sunlight-driven TiO_2/carbon dots photocatalyst: the significant roles of reactive oxygen species, Appl. Catal., B, 204 (2017) 250–259.
[37] G. Li, X. Nie, Y. Gao, T. An, Can environmental pharmaceuticals be photocatalytically degraded and completely mineralized in water using g-C_3N_4/TiO_2 under visible light irradiation-implications of persistent toxic intermediates, Appl. Catal., B, 180 (2016) 726–732.
[36] D. Komaraiah, E. Radha, J. Sivakumar, M.V. Ramana Reddy, R. Sayanna, Photoluminescence and photocatalytic activity of spin coated Ag^+ doped anatase TiO_2 thin films, Opt. Mater., 108 (2020) 110401, doi: 10.1016/j.optmat.2020.110401.
[38] J. Chen, Q. Yang, J. Zhong, J. Li, C. Burda, Microwave-assisted preparation of flower-like C_{60}/BiOBr with significantly enhanced visible-light photocatalytic performance, Appl. Surf. Sci., 540 (2021) 148340, doi: 10.1016/j.apsusc.2020.148340.
[38] L. Dou, X. Jin, J. Chen, J. Zhong, J. Li, Y. Zeng, R. Duan, One-pot solvothermal fabrication of S-scheme OVs-Bi_2O_3/Bi_2SiO_5 microsphere heterojunctions with enhanced photocatalytic performance toward decontamination of organic pollutants, Appl. Surf. Sci. 527 (2020) 146775, doi: 10.1016/j.apsusc.2020.146775.
[40] S. Lei, C. Yang, H. Liao, J. Chen, J. Zhong, J. Li, Enhanced photocatalytic activity of N_{134} carbon black modified Bi_2WO_6 benefited from ample oxygen vacancies and boosted separation of photoexcited carriers, Mater. Res. Bull., 133 (2021) 111075, doi: 10.1016/j.materresbull.2020.111075.

[41] L. Dou, Y. Xiang, J. Zhong, J. Li, S. Huang, Ionic liquid-assisted preparation of thin Bi_2SiO_5 nanosheets for effective photocatalytic degradation of RhB, Mater. Lett., 261 (2020) 127117, doi: 10.1016/j.matlet.2019.127117.
[42] M. Afzali, A. Mostafavi, T. Shamspur, Performance enhancement of perovskite solar cells by rhenium doping in nano-TiO_2 compact layer, Org. Electron., 86 (2020) 105907, doi: 10.1016/j.orgel.2020.105907.
[43] R.A.R. Monteiro, S.M. Miranda, C. Rodrigues-Silva, J.L. Faria, A.M.T. Silva, R.A.R. Boaventura, Vítor J.P. Vilar, Gas-phase oxidation of n-decane and PCE by photocatalysis using an annular photoreactor packed with a monolithic catalytic bed coated with P25 and PC500, Appl. Catal., B, 162 (2015) 66–74.
[43] V. Donchev, K. Kirilov, T. Ivanov, K. Germanova, Surface photovoltage phase spectroscopy-a handy tool for characterization of bulk semiconductors and nanostructures, Mater. Sci. Eng., B, 129 (2006) 186–192.
[44] H. Liu, C. Yang, J. Huang, Z. Deng, J. Zhong, J. Li, R. Duan, Carbon black decorated BiOCl with largely enhanced photocatalytic activity toward removal of RhB, Solid State Sci., 97 (2019) 105989, doi: 10.1016/j.solidstatesciences.2019.105989.
[45] J. Cao, X. Li, H. Lin, B. Xu, S. Chen, Q. Guan, Surface acid etching of $(BiO)_2CO_3$ to construct $(BiO)_2CO_3$/BiOX (X = Cl, Br, I) heterostructure for methyl orange removal under visible light, Appl. Surf. Sci., 266 (2013) 294–299.
[46] T. Cao, Y. Li, C. Wang, Z. Zhang, M. Zhang, C. Shao, Y. Liu, $Bi_4Ti_3O_{12}$ nanosheets/TiO_2 submicron fibers heterostructures: in situ fabrication and high visible light photocatalytic activity, J. Mater. Chem., 21 (2011) 6922–6927.
[47] D. Hou, X. Hu, P. Hu, W. Zhang, M. Zhang, Y. Huang, $Bi_4Ti_3O_{12}$ nanofibers-BiOI nanosheets p-n junction: facile synthesis and enhanced visible-light photocatalytic activity, Nanoscale, 5 (2013) 9764–9772.
[48] H. Li, J. Shi, K. Zhao, L. Zhang, Sustainable molecular oxygen activation with oxygen vacancies on the {001} facets of BiOCl nanosheets under solar light, Nanoscale, 6 (2014) 14168–14173.
[49] P. Wang, L. Ge, M. Li, W.P. Li, L. Li, Y.H. Wang, J.H. Yu, Photoelectrochemical sensor based on molecularly imprinted polymer-coated TiO_2 nanotubes for lindane specific recognition and detection, J. Inorg. Organomet. Polym. Mater., 23 (2013) 703–711.
[50] D. Ma, J. Zhong, R. Peng, J. Li, R. Duan, Effective photoinduced charge separation and photocatalytic activity of hierarchical microsphere-like C_{60}/BiOCl, Appl. Surf. Sci., 465 (2019) 249–258.
[51] M. Paszkiewicza, J. Łuczakb, W. Lisowskic, P. Patyka, A. Zaleska-Medynska, The ILs-assisted solvothermal synthesis of TiO_2 spheres: the effect of ionic liquids on morphology and photoactivity of TiO_2, Appl. Catal., B, 184 (2016) 223–237.
[52] M.A. Henderson, A surface science perspective on TiO_2 photocatalysis, Surf. Sci. Rep., 66 (2011) 185–297.
[53] H. Einaga, S. Futamura, T. Ibusuki, Heterogeneous photocatalytic oxidation of benzene, toluene, cyclohexene and cyclohexane in humidified air: comparison of decomposition behavior on photoirradiation TiO_2 catalyst, Appl. Catal., B, 38 (2002) 215–225.
[54] Y. Liu, R. Wang, Z. Yang, Enhanced visible-light photocatalytic activity of Z-scheme graphitic carbon nitride/oxygen vacancy-rich zinc oxide hybrid photocatalysts, Chin. J. Catal., 12 (2015) 2135–2144.
[55] H. Li, W. Li, S. Gu, Forming oxygen vacancies inside in lutetium-doped Bi_2MoO_6 nanosheets for enhanced visible-light photocatalytic activity, J. Mol. Catal., 433 (2017) 301–312.
[56] S. Wang, D. Chen, F. Niu, Hydrogenation-induced surface oxygen vacancies in $BiFeO_3$ nanoparticles for enhanced visible light photocatalytic performance, J. Alloys Compd., 688 (2016) 399–406.